



Development and application of reflection high-energy positron diffraction

A. Kawasuso ^{a,*}, S. Okada ^a, A. Ichimiya ^b

^a Japan Atomic Energy Research Institute, Takasaki Establishment, 1233 Watanuki, Takasaki, 370-1292, Japan

^b Department of Applied Physics, Nagoya University Chikusa-ku, Nagoya 464-8603, Japan

Received 21 October 1999

Abstract

Reflection high-energy positron diffraction (RHEPD) has been utilized using a 20 keV positron beam generated by an electrostatic beam apparatus. The structure of a hydrogen-terminated Si(1 1 1) surface has been analyzed from the rocking curves with dynamical calculation. Residual surface roughness observed after the hydrogen-termination was explained as the presence of SiH₃ molecule on monohydride surface. Reflectivities of positrons at Au, Ni and Ir(00 1) surfaces have been measured as a function of positron energy normal to surface. Abrupt decreases in the reflectivities were observed in the total reflection region of positrons, which are possibly associated with the surface dipole barriers. © 2000 Elsevier Science B.V. All rights reserved.

PACS: 61.14.Hg; 68.55.Jk

Keywords: Positron beam; Positron diffraction; Reflection high-energy positron diffraction (RHEPD); Surface; Hydrogen-terminated Si; Surface dipole barrier

1. Introduction

Reflection high-energy positron diffraction (RHEPD) is a powerful tool in the surface science [1,2]. This method is utilized by replacing electrons with positrons in reflection high-energy electron diffraction (RHEED). In 1993, Ichimiya [1] described a framework of RHEPD method based on the Bragg equation and further many-wave dy-

namical theory in light of the modern surface science. It is predicted that, in RHEPD experiment, total reflection of positrons below a critical angle and the first Bragg peak might be observed due to the positive crystal potential for positrons. These effects are unique for positrons and hence give rise to advantages of RHEPD method. The exchange interaction is absent in positron diffraction. In RHEPD analysis, correlation interaction is also negligible and inelastic processes, such as plasmon excitation, are reduced as compared to the case of low-energy positron diffraction (LEPD [3]). These facts make diffraction intensity analysis in RHEPD be much easier than that in LEPD.

* Corresponding author. Tel.: +81-27-346-9331; fax: +81-27-346-9687.

E-mail address: ak@taka.jaeri.go.jp (A. Kawasuso).

Ichimiya [1] suggested that surface-related physical parameters, such as coverage of adsorbed layer, the surface Debye temperature and surface roughness could be determined using the total reflection of positrons. Capabilities of reflectivity measurement for high-energy positrons to determine the surface dipole barrier of metals have already been argued by Oliva [4]. At present, only high-energy positron reflectivity measurement is thought to be able to provide the surface dipole barriers directly [4,5].

Since in RHEPD experiment positron beam is irradiated onto crystal surface at small glancing angles (several degrees), to observe diffraction patterns it is critical to form a positron beam with small angular divergence and diameter. It is therefore preferred to develop an electrostatic positron beam apparatus. In 1998, first clear RHEPD patterns were observed from a hydrogen-terminated Si(1 1 1) surface [2] after the first trial using a positron beam generated by an electron LINIAC [6]. The rocking curve for the specular spot was also determined. Differences between RHEPD and RHEED experiments were clearly evidenced from their rocking curves.

In this article, we describe the principle of RHEPD method, instrumentation with the first trial and applications of RHEPD to structural analysis of hydrogen-terminated Si(1 1 1) surfaces and positron reflectivity measurement for metal surfaces. Present issues and future trials are also discussed.

2. Principle of RHEPD

In RHEPD experiment, a positron beam with several tens of kilo-electron-volts is irradiated onto a surface at glancing angle of incidence and back-reflected positrons are observed as a diffraction pattern using a screen. The experimental alignment of RHEPD and the comparison with LEPD and transmission positron diffraction (TPD) are schematically shown in Fig. 1. These are just antithetic to transmission electron diffraction (TED), LEED and RHEED. The positron diffraction experiments are today available except TPD.

Since positrons have the same mass with electrons, positron diffraction may be described from

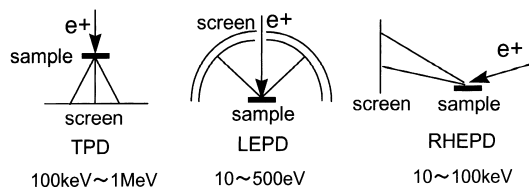


Fig. 1. Alignments of various positron diffraction experiments: (a) transmission positron diffraction; (b) low-energy positron diffraction; (c) reflection high-energy positron diffraction.

the analogy of electron diffraction. Difference from electron diffraction is that positrons are positively charged particle. Ichimiya [1] showed essential aspects of RHEPD as follows.

According to the Bragg equation, the diffraction condition is given by

$$E \sin^2 \theta = 37.5n^2/d^2 + eV_0, \quad (1)$$

where E is the energy of incident particle, θ the glancing angle, n the integer, d the atomic plane spacing and eV_0 is the inner potential. The inner potential is defined as the zeroth-order Fourier coefficient of the periodic crystal potential. Physically, the inner potential is the averaged electrostatic field felt by incoming fast charged particles. The magnitude is calculated by electron scattering factor given by Doyle and Turner [7]. Since for electrons the inner potential is negative, the primary Bragg peak ($n = 1$) is frequently unobserved in RHEED experiments. For example, in the case of Si(1 1 1), d and eV_0 are 3.14 Å and -12 eV, respectively, and hence, the primary Bragg peak does not appear because the left-hand side of Eq. (1) is negative. On the contrary, since the inner potential is positive for positrons, the primary Bragg peak might be observed. The intensities of lower order Bragg peaks are sensitive to surface potential more than higher order peaks. The appearance of the primary Bragg peak in RHEPD experiment gives rise to a surface sensitive diffraction pattern.

Positive inner potential for positrons may also result in total reflection of positrons below a critical glancing angle,

$$\theta = \arcsin \sqrt{eV_0/E}. \quad (2)$$

This equation is deduced from a condition that the positron energy normal to surface is equal to inner

potential: $E_{\perp} = E \sin^2 \theta = eV_0$ (in turn, $n = 0$ in Eq. (1)). That is, when the normal positron energy is less than the potential barrier, positrons are totally reflected without penetration. In the total reflection region, most positrons should be reflected at topmost surface. The reflectivity of positrons is fluctuated by the change in the surface potential.

The primary Bragg peak and total reflection in RHEPD are in other words explained as the effect of refraction. From the Snell's law, the glancing angle and the Bragg angle are connected by

$$\cos \theta_B / \cos \theta = \sqrt{E / (E - eV_0)}. \quad (3)$$

This relationship indicates that the refractive index for positrons is smaller than unity while for electrons it is greater than unity. Incident positrons penetrate into solids with smaller angles than glancing angles. Thus, positrons have a tendency to survey shallower layer than electrons.

Although the sensitivity of diffraction spots may be different between RHEPD and RHEED, patterns themselves are expected to be similar to each other in a sense that diffraction spots exhibit the reciprocal lattice rods of two-dimensional surface crystal. From the observed diffraction pattern, one can infer the surface state, e.g., cleanness, flatness, crystallized or amorphized and so on.

Detailed structural analysis of surface is allowed by the determination of rocking curve (diffraction spot intensity versus glancing angle plot) and comparison with theoretical curves assuming appropriate atomic models. Positrons strongly interact with nucleus and hence many waves are excited in their scattering process. Exact RHEPD rocking curves should be determined through dynamical computation [1,8].

3. Instrumentation

As mentioned already, conditions necessary for RHEPD experiment are (i) 10–100 keV positron beam in a non-magnetic field, (ii) positron beam with sufficiently small diameter (<1 mm) and angular divergence. The beam angular divergence

should be suppressed as small as possible (e.g., <0.1°) since typical RHEPD experiment is made at small glancing angles (<5°).

In this research, we adopted an electrostatic method so as to satisfy the above requirements. Fig. 2 shows the schematic overview of the apparatus. It is composed of a positron gun, three Einzel lenses separately shown in Fig. 3 and a sample chamber. At the end of the third Einzel lens, a deflector and a collimator are installed. Details of the positron gun and collimator are also drawn in Fig. 2. The positron gun, which was originally utilized by Canter et al. [9], is made from a positron source (^{22}Na , <5 mCi), a well-annealed tungsten moderator (5000 Å thick), an extraction grid, a Wehnelt electrode, a Soa tube and an anode. Positrons are accelerated up to 20 keV by floating the positron gun and the first Einzel lens electrostatically. At present, the anode is floated at +19.2 kV and moderator further floated by +800 V relative to the anode. The extraction grid is set to be +400 V relative to the anode, i.e., -400 V relative to the moderator. The Wehnelt and Soa are adjusted between 0 V and +400 V relative to the

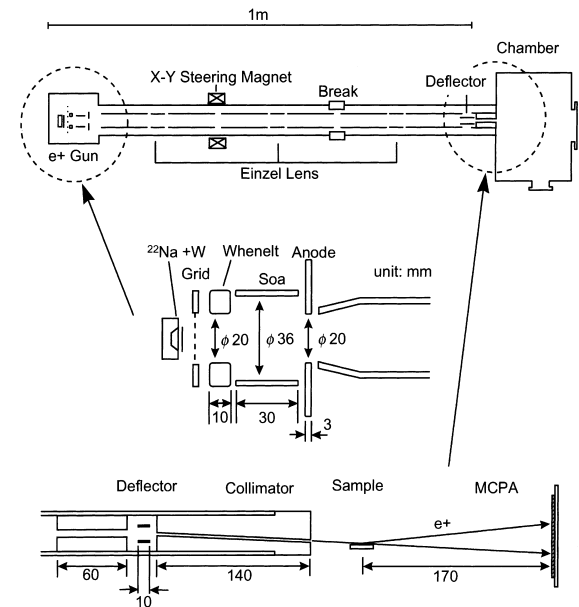


Fig. 2. Overview of the positron beam apparatus used in this study. Detailed plans of the positron gun and deflector + collimator is also shown (unit: mm).

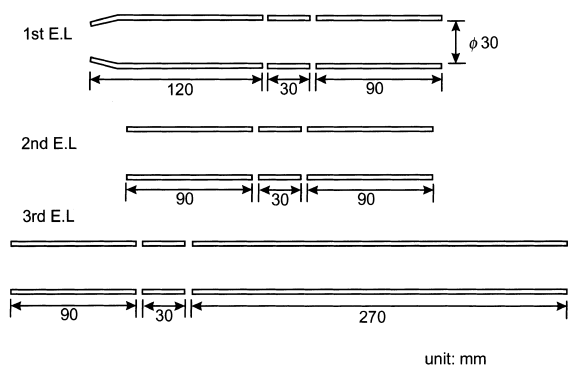


Fig. 3. Plans of Einzel lenses installed in the beam apparatus. The gap between electrodes is maintained to be 3 mm. Each lens is separated by 30 mm.

anode. The optimum combination of bias voltages for each part in the positron gun is determined so that final positron beam flux is maximized in practice. The first Einzel lens is floated at +9.6 kV and the last two are grounded.

The basic concept of the beam transportation is to set the focal point of each Einzel lens in front of the subsequent Einzel lenses. Indeed, from a numerical computation the beam trajectory is found to be optimized in this case [10]. However, strict focusing of the beam at sample position causes large angular divergence. This inhibits to form highly parallel beam which is suitable for RHEPD experiment. Thus, though the midpoint voltages of the former two Einzel lenses are set so that the beam is focused in front of the following lenses, that of the last Einzel lens is fixed at relatively weak value. The primary positron diameter (the source window) is approximately 5 mm. The beam diameter just after the third Einzel lens was measured to be 3–5 mm in the full width.

The Liouville's theorem requires that the product of energy E , diameter D and angular divergence θ_d of a beam should be constant:

$$D \sin \theta_d E^{1/2} = \text{const.} \quad (4)$$

from the conservation law of phase space volume [11]. The above relationship assures that if we select near-axis beam with relatively small diameter (e.g., <2 mm), accelerating thermal positrons with the energy of approximately 3 eV up to 20 keV, the

angular divergence could be sufficiently suppressed. In our experiment, the angular divergence of the final beam was under the detection limit, i.e., at least less than 1° . The outer axis beam always contains much aberrations. On the contrary, near axis-beam is highly parallel, more monochromatic, intensive and hence available. To select only near-axis beam, a long-length collimator ($\phi = 0.87$ mm, $l = 140$ mm) is installed after 3° deflection of the beam coming through the third Einzel lens. The maximum angle of the acceptance is approximately 0.36° . The energy spread of the final beam was approximately 200 eV (1%) for the average energy 20 keV. The beam flux is approximately 3000–5000 positrons/s.

The sample holder is placed just after the collimator with a mechanical rotator to change the glancing angle. Although in our early study the angular resolution was $\pm 0.5^\circ$, it is improved to be $\pm 0.1^\circ$ at present. Sample surface can be heated by infrared light illumination up to 1400°C . The sample chamber is evacuated at 10^{-10} – 10^{-9} Torr using a turbo molecular pump and an ion pump. The sample holder and the screen are separated by approximately 170 mm. Because of fairly weak beam flux, phosphor screens used in electron diffraction experiments are apparently unsuitable. We inserted a Hamamatsu micro-channel plate assembly (MCPA) with a phosphor plane (F2226-24P) instead of conventional screens. It was however impossible to observe any diffraction patterns as live images in human eyes. Phosphor screen images are then observed by a charge coupled device (CCD) camera connected to a personal computer and further accumulated as digital data. Considering the maximum gain of the MCPA is more than 10^6 , one may expect that one diffraction pattern can be obtained after several hours integration.

First successful RHEPD patterns were observed from a Si(111) surface cleaned by ultra pure water after HF dipping [2]. Fig. 4 shows the RHEPD patterns for $[1\bar{1}0]$ and $[1\bar{1}2]$ incidences at glancing angles of 4.5° and 4.0° , respectively. In these pictures, both specular and diffraction spots are clearly observed with shadow edges. A systematic dependence of diffraction patterns on the glancing angle and comparison with RHEED

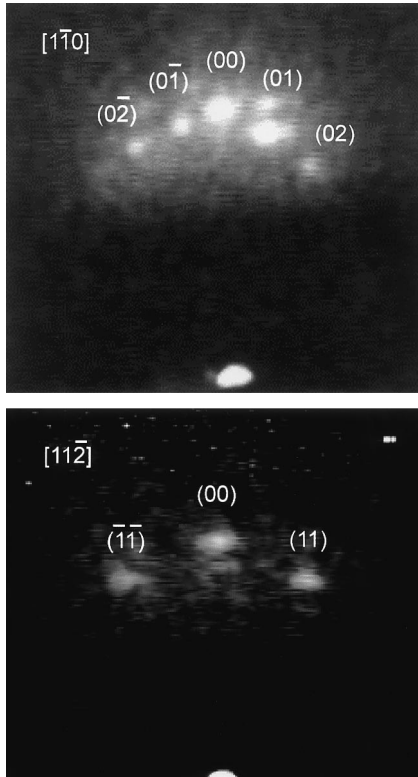


Fig. 4. First RHEPD patterns from a Si(111) surface cleaned by ultra pure water after HF dipping taken at the $[1\bar{1}0]$ and $[11\bar{2}]$ incidences at glancing angles of 4.5° and 4.0° , respectively. The energy of positron beam is 20 keV.

patterns are also reported [2]. The angle of diffraction spot is given by

$$\tan^2 \theta_{hk} = \frac{4\lambda^2}{3} \frac{(h^2 + hk + k^2)}{a^2}, \quad (5)$$

where θ_{hk} is the angle of the (hk) spot, λ the wavelength of incident particle and a is the lattice constant of surface lattice. The measured angles for diffraction spots are in good agreement with the calculated values using Eq. (5) with $a = 3.84 \text{ \AA}$ for unreconstructed Si(111) surface and nearly consistent with the RHEED pattern. Although in present RHEPD experiments zeroth Laue-zone is observable consistent with RHEED, the first Laue-zone have not yet been confirmed.

First RHEPD rocking curve for the specular beam [2] is shown in Fig. 5(a) with RHEED one

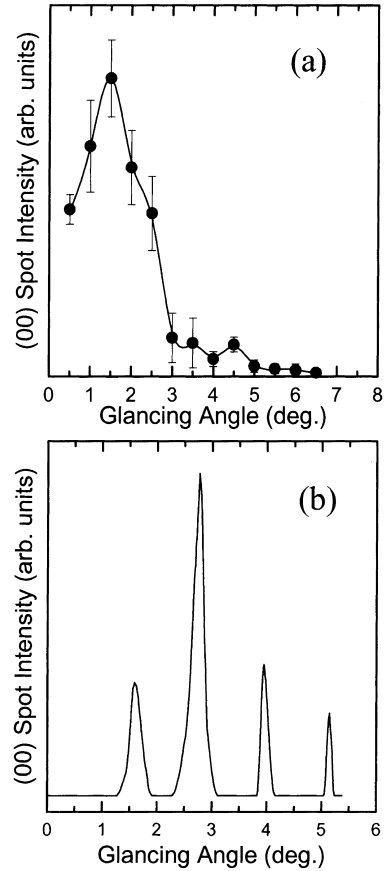


Fig. 5. (a) First RHEPD rocking curve from a Si(111) surface cleaned by ultra pure water after HF dipping at the $[1\bar{1}0]$ incidence. The energy of positron beam is 20 keV. The angular resolution is approximately $\pm 0.5^\circ$. (b) RHEED rocking curve for the similar sample at the $[1\bar{1}0]$ incidence. The energy of electron beam is 10 keV.

(Fig. 5(b)) taken by a 10 keV electron beam. No distinct fine structures are seen in the RHEPD rocking curve due to the low-angular resolution ($\pm 0.5^\circ$). However, it is clear that the specular beam intensity is considerably high below 2° and shows a peak at 1.5° . This behavior is explicitly explained as the primary Bragg peak and effect of total reflection. In Fig. 5(b), second to fifth Bragg peaks are seen. No primary Bragg peak and total reflection appear in RHEED experiment. Difference appear between RHEPD and RHEED is obvious from these figures.

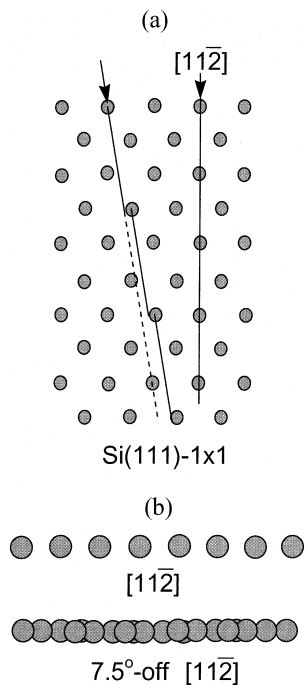


Fig. 6. (a) Top view of unreconstructed Si(111)-1 × 1 surface; (b) atomic arrangements of the surface seen from the $[1\bar{1}2]$ direction and in one-beam condition (7.5° – off from $[1\bar{1}2]$ direction).

We also examined so-called one-beam condition $[11,12]$ for full check of validity of this experiment. One-beam condition is that any diffraction spots except specular diminish at an asymmetric incidence. For Si(111) surface, it is 7.5° – off from a $[1\bar{1}2]$ direction. Fig. 6(a) illustrates the atomic arrangement of a Si(111)-1 × 1 surface. From a symmetric $[1\bar{1}2]$ incidence, the atoms are seen as discrete atomic rows as shown in Fig. 6(b). Changing the azimuth a little bit from a $[1\bar{1}2]$ axis, atoms are seen as shown in Fig. 6(c), like a continuous plate. As a result, in the one-beam condition, the transverse symmetry virtually vanishes and hence diffraction spots disappear. Fig. 7 shows the RHEPD patterns observed at the $[1\bar{1}2]$ incidence and the one-beam condition, respectively [13]. The diffraction spots observed in Fig. 7(a) are no longer observed in the one-beam condition in Fig. 7(b). This result is in good agreement with theory [11,12] suggesting the validity of the experiment.

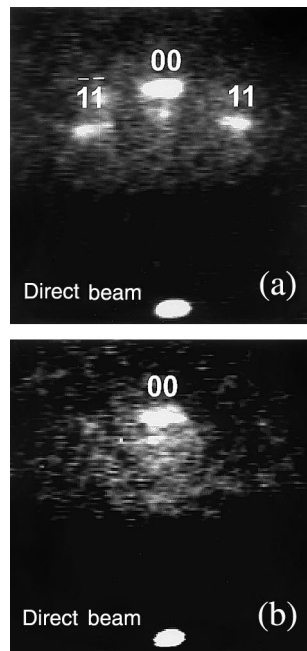


Fig. 7. The RHEPD patterns observed (a) at the $[1\bar{1}2]$ incidence and (b) in one-beam condition. The positron beam energy is 20 keV.

Thus, the above experimental results show the capabilities of RHEPD experiment in surface study. It is also revealed that diffraction pattern itself is similar in RHEPD and RHEED experiments except in RHEPD experiments the first Laue-zone has not yet been observed. Remarkable differences between RHEPD and RHEED appear in their rocking curves.

4. Applications of RHEPD

In this section, we report two instances of RHEPD experiments that we have carried out so far. One is structural analysis of hydrogen-terminated Si(111) surface [13] and the other is the measurements of surface dipole barriers of metallic crystals.

4.1. Hydrogen-terminated Si(111) surface

It is well known that Si(111) surfaces terminated with atomic hydrogen are highly stable for

oxidation and impurity contamination for sufficiently long period. This owes to the passivation of surface dangling bonds. Hydrogen-termination of Si surfaces is a current topic in the surface science because of its importance both in fundamentals and industry [14]. Hydrogen-terminated Si surfaces have been extensively studied with many approaches such as infrared absorption measurement [15–18], scanning tunneling microscope (STM) observation [19–24], ultraviolet photoelectron spectroscopy (UPS) [25] and electron diffraction experiments [26,27]. In view of this situation, it is interesting to investigate what RHEPD can evaluate for hydrogen-terminated Si(111) surfaces.

One effective way to obtain atomically flat hydrogen-terminated Si(111) surface is the boiling in ultra pure water [18] or the etching with NH_4F solution [20,24] or pH-controlled buffered HF solution [17] after HF dipping. In this study, we performed RHEPD experiments for NH_4F -prepared Si(111) surfaces.

Specimens were cut from a commercial Si(111) wafer oriented [112] and [110] directions. After degreasing treatment, they were subjected to oxidation by HNO_3 boiling and stripping the oxide layer by HF dipping for three times. Then, they were finished in NH_4 solution (0°C) for 20 min. As reported in the previous researches [17,18], the present samples exhibit a strong infrared absorption peak at 2084 cm^{-1} related to Si–H local vibration. The absorption band due to Si– H_3 was however difficult to observe. From atomic force microscopy observation, it was revealed that the step density of the surface is much reduced and average roughness was less than a few angstroms.

The RHEPD diffraction patterns showed no fractional order spots. This suggests that the surface holds a 1×1 structure as proposed through low-energy electron diffraction experiments [26]. Fig. 8 shows the RHEPD rocking curves for different azimuth. From the [112] incidence, the first to fifth Bragg peaks are observed at 1.4° , 2.2° , 2.8° , 3.5° and 4.3° . The higher order Bragg peaks were not observed in the previous RHEPD experiments because of the low-angular resolution. The positions of the observed peaks are in good agreement with those calculated from Eq. (1) with $eV_0 = +12$

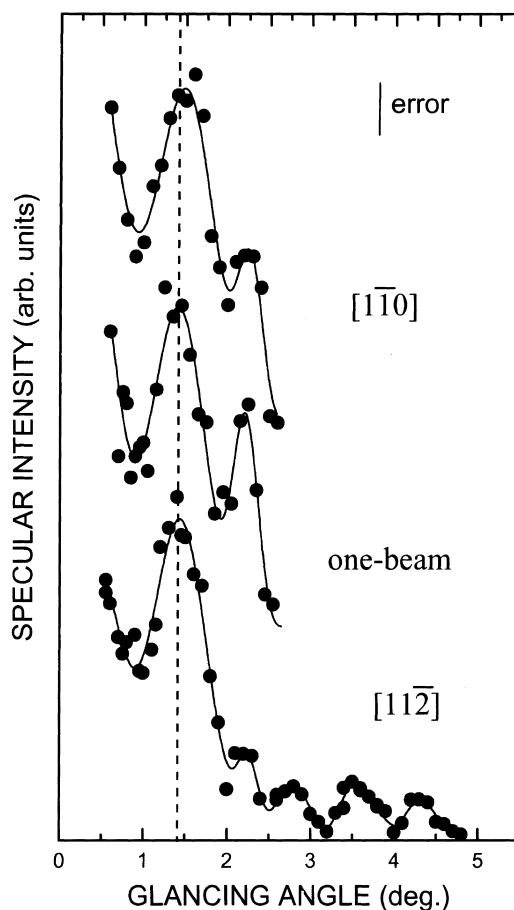


Fig. 8. The RHEPD rocking curves from a hydrogen-terminated Si(111) surface finished with NH_4F solution at the [112] and [110] incidences and in one-beam condition. The critical angle of the total reflection is shown by broken line (1.4° from Eq. (2)). The energy of positron beam is 20 keV. The angular resolution is $\pm 0.1^\circ$.

eV. This suggests that the absolute value of the inner potential for positrons are close to that for electrons. It is found that in the total reflection region distinct dip structure appear independent of azimuth. The dip structures suggests the change in the surface potential from the bulk-truncated surface potential.

To clarify the origin of the observed structures in the total reflection region, dynamical calculation including five beams has been performed for several surface models as shown in Fig. 9. The results of the computation are shown in Fig. 10. As

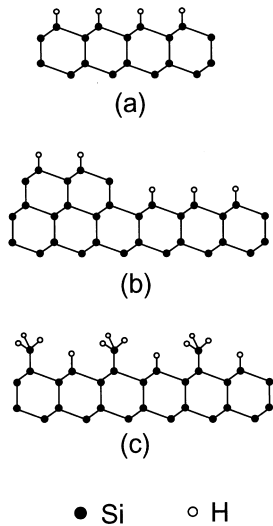


Fig. 9. Structural models of hydrogen-terminated Si(111) surface examined in numerical calculation: (a) an ideally hydrogen-terminated flat Si(111); (b) a monohydride Si(111) surface containing bilayer roughness; (c) a monohydride Si(111) surface on which SiH₃ molecule remain. The bond lengths of Si–Si and Si–H are fixed to be 2.35 and 1.2 Å, respectively.

mentioned above, the infrared absorption measurement and atomic force microscope observation imply that the prepared surface is mostly terminated with monohydride and atomically highly flat. The existence of adsorbed layer on a surface may result dip structures in the total reflection region because of the double barrier at the surface. Therefore, we first examined ideally hydrogen-terminated flat surface in Fig. 9(a). However, obviously, the observed dip structure is not reproduced in this model. It is concluded that the dip structure is not due to the effect of hydrogen. Probably, hydrogen atoms on Si surface act as only weak scattering centers due to the small atomic form factor compared to that of Si.

To reproduce the observed rocking curves, one may suppose imperfections of the surface. Considering residual roughness measured by atomic force microscopy, we further examined bilayer roughness and adsorption of Si–H₃ molecule on monohydride surface as shown in Fig. 9(b) and (c), respectively. Fig. 10(b) and (c) show that these surfaces exhibit dip structures in the total reflection region. Comparing the dip positions and line

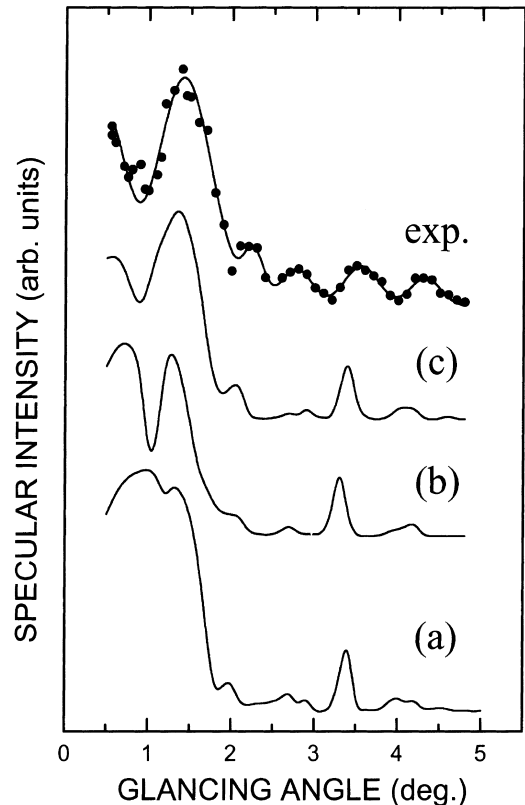


Fig. 10. Calculated rocking curves at the $[11\bar{2}]$ incidence for each models illustrated in Fig. 9. The coverage of bilayer roughness (model (b)) and SiH₃ molecule (model (c)) are assumed to be 0.4 and 0.2, respectively. The experimental result is also shown for comparison.

shapes between calculation and experiment, the model (c) closely matches the observation. Accordingly, the obtained RHEPD rocking curve indicates the presence of Si–H₃ molecule on the surface.

The model (c) is partially consistent with the infrared absorption measurement in which Si–H local vibration was found. However, absorption band related to Si–H₃ was under the detection limit in this study. Possibly, the oscillator strength of Si–H₃ is fairly weaker than that of Si–H. To observe infrared absorption peaks from Si–H₃ much highly precise measurements might be necessary. The existence of Si–H₃ molecule has not been evidenced for NH₄F-prepared Si(111) surfaces even in the STM observation [19,20,24].

However, this RHEPD study implies the existence of Si–H₃ with Si–H on NH₄F-prepared Si(111) surfaces.

From the RHEPD rocking curve analysis especially in the total reflection region, it is possible to guess detailed surface structure. In the above example, we proposed a new structural model. An important point is that such a proposal has not been made from conventional spectroscopy and microscopy.

4.2. Measurement of surface dipole barriers of metals

In this section, we report the reflectivity measurement of high-energy positrons for Au(001), Ni(001) and Ir(001) surfaces. Specular spot intensities for these surfaces were found to decrease suddenly with the threshold energies. The abrupt drops in the reflectivities may be attributed to the effect of the surface dipole barriers as predicted by Oliva [4].

The work function of a metal is defined as the minimum energy to remove an electron from deep in the metal to vacuum. An electrically polarized layer is formed at the topmost surface of a metal due to the spilling of free electrons resulting the dipole barrier D . The work function is given by

$$\phi_- = -D + \mu, \quad (6)$$

where μ is the chemical potential of an electron. The above situation is schematically shown in Fig. 11. The chemical potential is determined as purely bulk electronic property, i.e., the sum of kinetic energy ($k_F^2/2$) and exchange-correlation energy

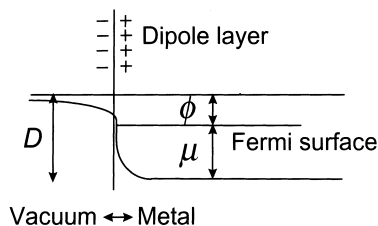


Fig. 11. Schematic energy diagram of a metal in the jellium approximation. The vertical and horizontal axes represent energy and depth, respectively, of the metal ($z < 0$: vacuum, $z > 0$: interior of the metal).

(ϵ_{xc}). To evaluate the work function, it is necessary to know the values of both D and μ . Lang and Kohn [28] calculated these values numerically based on the jellium approximation that hypothesized a uniform positive background instead of the discrete ion distribution. They determined the electron distribution and thereby surface dipole barrier. For simple metals (Li, Na, K, Rb, Cs, Al, Pb, Zn and Mg), the calculated work functions are in good agreement with experimental values. Whereas, for noble metals (Au, Ag and Cu), the discrepancy between the theory and experiments are relatively large. Heine and Hodges [29] and Hodges and Heine [30] also calculated the dipole barriers for several simple metals and also noble metals using the experimental cohesive energies and work functions. Alonso and Iniguez [31] deduced the surface dipole barriers using the experimental work functions and theoretical chemical potentials calculated by the augmented spherical wave method.

The work function can be determined directly in experiments. The obtained values are thus comparable with theoretical evaluations. The independent determination of the dipole barrier and/or chemical potential is strongly desired to check the validity of electronic theories. Oliva [4] proposed an idea to use positron reflectivity measurement to determine the surface dipole barrier. The essence of his idea is that positive particle like a positron will be repelled from a metallic surface by the dipole barrier. As the energy of incoming positrons (E) increases, the reflectivity may abruptly decrease at above $E = D$ giving a direct measurement of D . Since typical plasmon energy is approximately 15 eV, the screening effect, the correlation interaction and also inelastic particle–electron scattering process are not negligible for low-energy positrons (< 10 eV). These effects apparently modulate the “true” barrier height.

Mayer et al. [32] attempted to determine the surface dipole barriers for Ni(110) and Cu(100) by changing incident energy of positrons from 50 to 400 eV at fixed glancing angles. Although the energy E is high enough to diminish attractive correlation interaction, the reflectivity versus normal positron energy plots showed somewhat broad features. They interpreted the results as the

broadening of barrier height by inelastic processes. It is suitable to use high-energy positrons (more than several tens of kilo-electron-volts) in the glancing incidence.

For the measurement of the surface dipole barriers, the normal positron energy may be varied at around several electronvolts. Since the normal component of positron energy to a surface is given by $E_{\perp} = E \sin^2 \theta$ with the incident energy E and the glancing angle θ , suitable glancing angle is $0.5\text{--}2.0^{\circ}$ for $E = 20$ keV. It is intriguing to apply the RHEPD technique to the positron reflectivity measurement at metal surfaces.

Specimens used in this study are Au(001), Ni(001) and Ir(001) single crystals. The surfaces of the former two specimens were chemically polished with the miss-orientation and roughness less than 0.25° and 0.03μ , respectively. The Ir(001) specimen was grown on a MgO(001) substrate by the electron beam evaporation technique. The surfaces were heated by infrared light flashing for several times in the chamber evacuated below 7×10^{-10} Torr.

Fig. 12(a)–(c) shows the specular intensity of positrons as a function of normal positron energy for each specimen. It is found that after the slight increases the specular intensities reach a maximum and then steeply decrease. The threshold energies for the steep drops of the specular intensities are determined to be 4.5 ± 0.5 , 6.3 ± 0.7 and 13.9 ± 1.4 eV for Au, Ni and Ir, respectively. These abrupt drops of the specular intensities indicate the existence of repulsive barriers for positrons at near surface region. This implies that the observed steep decreases in the specular intensities may be due to the repulsion of positrons mainly by the surface potentials. The threshold energies are therefore inferred to correspond to the potential height. Although the increases in the intensities before the steep drops are not clear at present, one of the possible explanations is the capture of positrons at the depression potential just outside the surface so that positrons can propagate along the surface (i.e., surface trapped positrons) and/or can form positronium atoms [33].

As mentioned above, the positron reflectivity decreases suddenly at above $E_{\perp} = D$ [4]. Thus, the observed threshold effect for the specular intensi-

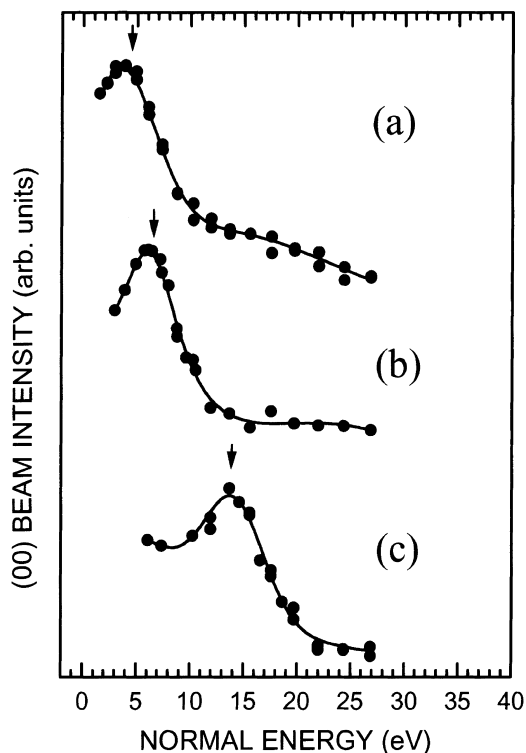


Fig. 12. The specular intensities of positrons as a function of normal positron energy for (a) Au, (b) Ni and (c) Ir. The intensities are collected by dividing with a geometrical factor $\sin \theta$.

ties may be attributed to the repulsion of positrons from the surface dipole barriers.¹ Based on the jellium approximation, Lang and Kohn [28] calculated the surface dipole barrier as a function of electron density parameter r_s , where r_s is defined by $4\pi r_s^3/3 = 1/n$ with the average electron density n . These values are shown in Fig. 13 with the threshold energies for Au ($r_s = 3.01$), Ni ($r_s = 1.83$) and Ir ($r_s = 1.38$) obtained above. The result of the jellium model shows that the surface dipole barrier increases with decreasing r_s (increasing average electron density).

¹ The inner potential of Au, Ni and Ir are estimated to be 26.4, 25.5 and 38.1 eV, respectively. These are significantly higher than the observed threshold energies. Thus, the threshold effect may be due to the repulsion of positrons by the surface potentials and not by the inner potentials.

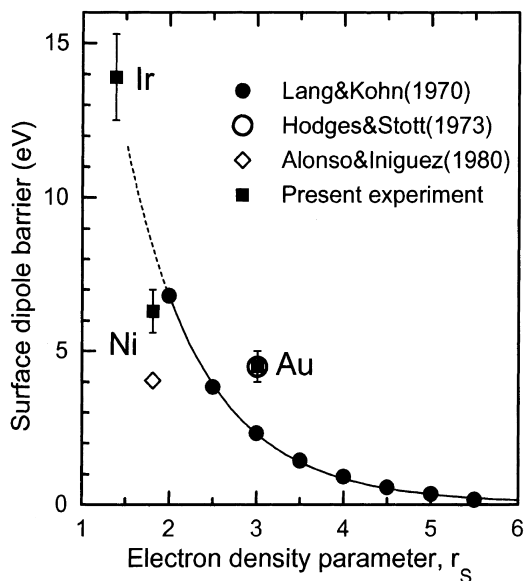


Fig. 13. Surface dipole barriers of metals calculated by the jellium approximation (solid line) and its extrapolation (broken line), semi-empirical estimation for Au and Ni (open circles) with the threshold energies for Au, Ni and Ir obtained from Fig. 12 as a function of electron density parameter r_s defined by $4\pi r_s^3/3 = 1/n$ with the average electron density n .

Although the experimental results are in agreement with this trend, the quantitative agreement seems to be inadequate. The jellium model successfully calculates the work functions for simple metals which have only s and p valence electrons. However, for noble metals, the results of the jellium model significantly deviate from experimental values. It is pointed out that the s - d hybridization should be taken into account in the calculation for noble metals. Possibly, the discrepancy between the jellium model and the experimental point for Au shown in Fig. 13 is arising from the above reasons. Similarly, the jellium model may not be suitable for Ni, which is a transition metal and also Ir.

Hodges and Heine [30] calculated the surface dipole barriers in a semi-empirical manner considering the effect of s - d hybridization. The calculated value for Au are also shown in Fig. 13. The threshold energy for Au is in good agreement with the surface dipole barriers collected by the semi-empirical method. The calculated surface dipole

barrier for Ni by Alonso and Iniguez [31] is 4.04 eV. A similar value is obtained using the chemical potential for electrons by Boev et al. [34]. The experimental threshold energy for Ni is somewhat higher than the theoretical values. The surface dipole barrier is thought to be sensitive to the surface state, such as the lattice relaxation and adsorption effects. Considering that the theoretical estimates are made for ideal flat surfaces, the above discrepancy may reflect the detailed surface state.

It should be noted that the threshold effect of the positron reflectivity, which were not clearly seen in the previous study using low-energy positrons, were observed for Au, Ni and Ir. The above results indicate that positron reflectivity measurement might provide surface dipole barriers of metals. Although the measured threshold energies are comparable to theoretical surface dipole barriers, for more detail studies it is wished to accumulate experimental data using various metals.

5. Summary

In summary, RHEPD experiments have been demonstrated using a positron beam generated in an electrostatic beam apparatus. Taking advantage that reflectivity of high-energy positrons at glancing of incidence is sensitive to the surface potential in the total reflection region, we investigated hydrogen-terminated Si(1 1 1) surfaces and several metal surfaces. The results of these applications strongly imply the potential of RHEPD in the surface science. In particular, comparing experimental and theoretical rocking curves, a new structural model for hydrogen-terminated Si(1 1 1) surfaces was proposed. Possibility of positron reflectivity measurement to determine surface dipole barriers of metals was also examined.

In this study, the first Laue-zone and fractional order spots which are easily observed in electron diffraction experiments have not been observed. Most important applications of RHEPD, such as the measurement of the surface Debye temperature and the structural analyses of adsorbed layers have not yet been taken place. Many open questions still remain about physics of interaction between high-energy positrons and solid surfaces. To

attack the existing problems, however, it should be stated that the quality of the positron beam should be improved more up to the comparable level with conventional electron beam in their energy spread, angular divergence, brightness and so on, as much as possible. The construction of the second generation RHEPD apparatus is strongly desired to make present issues be clear.

Acknowledgements

The authors thank K. Kojima, M. Yoshikawa and S. Yamamoto of Japan Atomic Energy Research Institute for their helps in optical measurement, AFM observation and providing an Ir crystal, respectively. We are also grateful to H. Nakahara of Nagoya University for his help in making RHEED experiments.

References

- [1] A. Ichimiya, *Solid State Phenom.* 28/29 (1992/93) 143.
- [2] A. Kawasuso, S. Okada, *Phys. Rev. Lett.* 81 (1998) 2695.
- [3] K.F. Canter, C.B. Duke, A.P. Mills, in: R. Vanselow, R. Hoew (Eds.), *Chemistry and Physics of Solid Surface*, vol. VIII, Springer, Berlin, 1990, p. 183.
- [4] J. Oliva, Ph. D. thesis, University of California, San Diego, CA, 1979, unpublished.
- [5] P.J. Schultz, K.G. Lynn, *Rev. Mod. Phys.* 60 (1988) 701.
- [6] I. Kanazawa, Y. Itoh, M. Hirose, H. Abe, O. Sueoka, S. Takamura, A. Ichimiya, Y. Murata, F. Komori, K. Fukutani, S. Okada, T. Hattori, *Appl. Surf. Sci.* 85 (1995) 124.
- [7] P.A. Doyle, P.S. Turner, *Acta Cryst. A* 24 (1968) 390.
- [8] A. Ichimiya, *Jpn. J. Appl. Phys.* 22 (1983) 176.
- [9] K.F. Canter, P.H. Lippel, W.S. Crane, A.P. Mills Jr., in: A. P. Mills Jr., W.S. Crane, K.F. Canter (Eds.), *Positron Studies of Solids, Surfaces, and Atoms*, World Scientific, Singapore, 1986, p. 199.
- [10] K. Fujimori, unpublished.
- [11] A. Ichimiya, *Surf. Sci.* 192 (1987) L893.
- [12] A. Ichimiya, in: S.Y. Tong, M.A. Van Hove, K. Takayanagi, X.D. Xie (Eds.), *The Structure of Surfaces*, III, Springer, Berlin, 1991, p. 162.
- [13] A. Kawasuso, M. Yoshikawa, K. Kojima, S. Okada, A. Ichimiya, *Phys. Rev. B* 61 (2000) 2102.
- [14] T. Ohmi, *J. Electrochem. Soc.* 143 (1996) 2957.
- [15] V.A. Burrows, Y.J. Chabal, G.S. Higashi, K. Raghavachari, S.B. Christman, *Appl. Phys. Lett.* 53 (1988) 998.
- [16] Y.J. Chabal, G.S. Higashi, K. Raghavachari, V.A. Burrows, *J. Vac. Sci. Technol. A* 7 (1989) 2104.
- [17] G.S. Higashi, Y.J. Chabal, G.W. Trucks, K. Raghavachari, *Appl. Phys. Lett.* 56 (1990) 656.
- [18] S. Watanabe, N. Nakayama, T. Ito, *Appl. Phys. Lett.* 59 (1991) 1458.
- [19] R.S. Becker, G.S. Higashi, Y.J. Chabal, A.J. Becker, *Phys. Rev. Lett.* 65 (1990) 1917.
- [20] H. Tokumoto, Y. Morita, K. Miki, *Mat. Res. Soc. Symp. Proc.* 259 (1992) 409.
- [21] Y. Morita, N. Miki, H. Tokumoto, *Appl. Phys. Lett.* 59 (1991) 1347.
- [22] Y. Morita, N. Miki, H. Tokumoto, *Appl. Surf. Sci.* 60/61 (1992) 466.
- [23] Y. Morita, N. Miki, H. Tokumoto, *Ultramicroscopy* 42-44 (1992) 922.
- [24] Y. Morita, H. Tokumoto, *Mat. Res. Soc. Symp. Proc.* 315 (1993) 491.
- [25] K.C. Pandey, T. Sakurai, H.D. Hagstrum, *Phys. Rev. Lett.* 35 (1975) 1728.
- [26] P.H. Hahn, *Mat. Res. Soc. Symp. Proc.* 54 (1986) 645.
- [27] A. Ichimiya, S. Mizuno, *Surf. Sci. Lett.* 191 (1987) L765.
- [28] N.D. Lang, W. Kohn, *Phys. Rev. B* 3 (1971) 1215.
- [29] V. Heine, C.H. Hodges, *J. Phys. C* 5 (1972) 225.
- [30] C.H. Hodges, V. Heine, *Phys. Rev. B* 7 (1973) 73.
- [31] J.A. Alonso, M.P. Iniguez, *Solid State Commun.* 33 (1980) 59.
- [32] R. Mayer, C.S. Zhang, K.G. Lynn, J. Throwe, P.M. Marcus, D.W. Gidley, F. Jona, *Phys. Rev. B* 36 (1987) 5659.
- [33] A. Ishii, T. Aisaka, *Appl. Surf. Sci.* 85 (1995) 33.
- [34] O.V. Boev, M.J. Puska, R.M. Nieminen, *Phys. Rev. B* 36 (1987) 7786.